Atmos. Chem. Phys., 24, 5823–5835, 2024
https://doi.org/10.5194/acp-24-5823-2024

Atmospheric Chemistry and Physics
Open Access
EGU

Rapid iodine oxoacid nucleation enhanced by dimethylamine in broad marine regions

Haotian Zu[1], Biwu Chu[2], Yiqun Lu[3], Ling Liu[1], and Xiuhui Zhang[1]

[1]Key Laboratory of Cluster Science, Ministry of Education of China, School of Chemistry and Chemical Engineering, Beijing Institute of Technology, Beijing 100081, China
[2]State Key Joint Laboratory of Environment Simulation and Pollution Control, Research Center for Eco-Environmental Sciences, Chinese Academy of Sciences, Beijing 100085, China
[3]State Environmental Protection Key Laboratory of Formation and Prevention of Urban Air Pollution Complex, Shanghai Academy of Environmental Sciences, Shanghai 200233, China

Correspondence: Ling Liu (lingliu@bit.edu.cn) and Xiuhui Zhang (zhangxiuhui@bit.edu.cn)

Received: 2 August 2023 – Discussion started: 17 October 2023
Revised: 24 February 2024 – Accepted: 24 March 2024 – Published: 22 May 2024

Abstract. Recent experiments have revealed a vital nucleation process of iodic acid (HIO_3) and iodous acid (HIO_2) under marine boundary layer conditions. However, HIO_3–HIO_2 nucleation may not effectively drive the observed rapid new particle formation (NPF) in certain coastal regions influenced by urban air masses. Dimethylamine (DMA) is a promising basic precursor to enhance nucleation considering its strong ability to stabilize acidic clusters and the wide distribution in marine atmosphere, while its role in HIO_3–HIO_2 nucleation remains unrevealed. Hence, a method combining quantum chemical calculations and Atmospheric Cluster Dynamics Code (ACDC) simulations was utilized to study the HIO_3–HIO_2–DMA nucleation process. We found that DMA can preferentially accept the proton from HIO_3 as a basic precursor in the most stable configurations of HIO_3–HIO_2–DMA clusters. Kinetically, the participation of DMA in the cluster formation pathways of the iodine oxoacid system could be significant at the 10^{-1} to 1 pptv level of [DMA]. Furthermore, DMA can enhance the cluster formation rates of the HIO_3–HIO_2 system in marine and polar regions near DMA sources more than 10^3-fold. Compared to the classical nucleation mechanism, the HIO_3–HIO_2–DMA mechanism exhibits strong nucleation ability, worthy of consideration as a promising mechanism in marine and polar regions rich in amine sources. The newly proposed HIO_3–HIO_2–DMA ternary mechanism might provide an explanation for some missing fluxes of atmospheric iodine particles.

1 Introduction

Atmospheric aerosols, the intricate suspension formed by fine particles in the atmosphere, exert far-reaching influences on global climate (Haywood and Boucher, 2000; Murphy and Ravishankara, 2018; Lee et al., 2019), radiation balance (Haywood and Boucher, 2000), and human health (Pope and Dockery, 2006; Gong et al., 2014). A significant source of atmospheric aerosols on the worldwide scale is the new particle formation (NPF), encompassing nucleation and subsequent growth (Zhang, 2010). Nucleation is identified as the key process of NPF events. Therefore, understanding the nucleation mechanism is vital for comprehending the behavior of aerosols (Zhang et al., 2012; Kalivitis et al., 2015).

Sulfuric acid (H_2SO_4) is considered a crucial precursor for the nucleation in continental regions. However, under actual atmospheric conditions, the H_2SO_4–water (W) binary nucleation is far from sufficient to explain the observed strong NPF events (Elm, 2021a). Therefore, additional components are essential for nucleation. Specifically, abundant atmospheric bases, such as ammonia (A) and alkylamines (methylamine (MA), dimethylamine (DMA), trimethylamine (TMA), and ethylenediamine (EDA); Weber et al., 1996; Kurtén et al., 2008; Kirkby et al., 2011; Elm

et al., 2017; Xie and Elm, 2021), are recognized as important stabilizers for H_2SO_4-driven nucleation. Computational work by Kurtén et al. (2008) and experimental studies by Almeida et al. (2013) indicated that, despite the lower atmospheric concentration of DMA (a few parts per trillion by volume), the promoting effect of DMA on the H_2SO_4-driven nucleation rate is several orders of magnitude higher than that of A. Moreover, nitric acid (NA) is also a potential precursor in the nucleation process (Knattrup and Elm, 2022). Liu et al. (2018, 2021a) showed the significant promoting effect of NA on the classical H_2SO_4–A and H_2SO_4–DMA nucleation mechanisms by theoretical methods. Additionally, Wang et al. (2020) studied the nucleation process of mixed vapor of NA and A under atmospheric conditions in the Cosmics Leaving OUtdoor Droplets (CLOUD) chamber at the European Organization for Nuclear Research and subsequently considered the promoting effect of H_2SO_4 on the NA–A system (Wang et al., 2022).

Given the vast expanses of the ocean, marine aerosols play an indispensable role in the global aerosol system (O'Dowd and de Leeuw, 2007). H_2SO_4 and methanesulfonic acid (MSA), the oxidation products of dimethylsulfide (DMS), are considered to be important nucleation precursors over the oceans (Elm, 2021b). Theoretical calculations (Chen et al., 2020a, b; Shen et al., 2020) have indicated that basic precursors such as A, MA, and DMA can promote MSA-based nucleation processes. However, a recent study on aerosol acidity showed that global models substantially overestimate the concentrations of A, especially in polar regions (Nault et al., 2021). This may slightly weaken the influence of H_2SO_4-based and MSA-based nucleation in marine atmosphere (He et al., 2023). In recent years, iodine species, originating from biological emissions of marine macroalgae (O'Dowd et al., 2002c, b, 2002a; Zhang et al., 2012), have also been thought to be important precursors of the frequent NPF events in marine and polar regions (Hoffmann et al., 2001; Ehn et al., 2010; McFiggans et al., 2010; Mahajan et al., 2011; Baccarini et al., 2020). Several studies have consistently highlighted the pivotal role of iodic acid (HIO_3) in marine nucleation processes (Yu et al., 2019; Baccarini et al., 2020; Rong et al., 2020; Xia et al., 2020; He et al., 2021; Sipilä et al., 2016). Molecular-level observations conducted at the Mace Head coastal station in Ireland have provided evidence that the nucleation process is predominantly driven by HIO_3 with a high concentration of 10^8 molecules cm^{-3} (Sipilä et al., 2016). Iodous acid (HIO_2) was also detected in both gas (up to 2×10^6 molecules cm^{-3}) and particle phases during the NPF events together with the HIO_3 (Yu et al., 2019; Sipilä et al., 2016). Recently, HIO_2 has been confirmed to play an important role in stabilizing the neutral HIO_3 clusters in the Cosmics Leaving OUtdoor Droplets (CLOUD) chamber at the European Organization for Nuclear Research (CERN) (He et al., 2021). This was found to be concerned with the base-like behavior of HIO_2 in HIO_3–HIO_2 clusters by subsequent theoretical studies (Zhang et al., 2022a; Liu et al., 2023). In short, the iodine oxoacids (HIO_x, $x = 2, 3$) can drive rapid particle formation, and they may play an important role in marine and polar NPF process. However, in certain coastal areas influenced by urban air masses, such as the Zhejiang region, former studies have indicated that iodine species could drive nucleation processes, while the HIO_3–HIO_2 nucleation mechanism may not sufficiently explain the field observation results (Yu et al., 2019; Ma et al., 2023; Zu et al., 2024; Xia et al., 2020), which indicates that other nucleation precursors may be involved.

In addition to iodine species, dimethylamine (DMA) is also a common nucleation precursor in the oceanic atmosphere (Facchini et al., 2008). DMA can originate from plankton and bacteria in seawater (Müller et al., 2009; Hu et al., 2015; Chen et al., 2021). Ice-influenced ocean may also be an important source of DMA (Dall'Osto et al., 2017, 2019). Moreover, industrial activities also generate a large amount of DMA-containing pollutants (Corral et al., 2022). Hence, DMA is widely distributed and abundant under the different oceanic atmospheric conditions, displaying a spatial distribution remarkably akin to that of iodine species in mid-latitude coastal and high-latitude polar regions (Vanneste et al., 1987; Gronberg et al., 1992; Gibb et al., 1999; Quéléver et al., 2022). DMA has a strong base-stabilization effect on the H_2SO_4-based nucleation process (Almeida et al., 2013; Yao et al., 2018) since it possesses relatively strong basicity. Therefore, DMA may participate in and facilitate the iodine oxoacid nucleation through similar acid-base interactions with the H_2SO_4–DMA system. However, previous studies have not adequately explored the influence of DMA on iodine oxoacid (HIO_3 and HIO_2) nucleation in marine regions, and the ternary nucleation mechanism of HIO_3–HIO_2–DMA remains to be disclosed.

In the present study, the nucleation mechanism of HIO_3–HIO_2 enhanced by DMA under atmospheric conditions of different marine regions (mid-latitude coastal and high-latitude polar regions) was studied by a method combining quantum chemical calculation and the Atmospheric Cluster Dynamics Code (ACDC) model. The simulated system contains $(HIO_3)_x \cdot (HIO_2)_y \cdot (DMA)_z$ ($1 \le x+y+z \le 6$; $x+y \ge z$) clusters. The largest clusters with a mobility diameter (Almeida et al., 2013) up to 1.3 nm in the size range of nucleation clusters (Zhang et al., 2012) are stable enough to resist evaporation at the studied temperature, and clusters with more DMA molecules ($x + y < z$) are usually unstable. This study aims to reveal the potential role of DMA in the HIO_3–HIO_2 nucleation and help to better understand the intensive NPF events in broad marine regions.

2 Method

2.1 Quantum chemical calculations

The HIO_3–HIO_2–DMA system is composed of ternary clusters (HIO_3–HIO_2–DMA), binary clusters (HIO_3–HIO_2,

HIO_3–DMA, HIO_2–DMA), and pure-HIO_x ($x = 2$, 3) clusters. The most stable configurations of HIO_3–HIO_2–DMA ternary clusters and HIO_2–DMA binary clusters were proposed in this study for the first time. Additionally, the structures of HIO_3–HIO_2–DMA clusters and pure-HIO_x ($x = 2$, 3) clusters presented in this work were adopted from the stable configurations with the lowest Gibbs free energy of formation in previous studies (Rong et al., 2020; Ning et al., 2022; Zhang et al., 2022b; Liu et al., 2023) at the same level of theory. A multi-step searching process that can systematically screen the structures of clusters was adopted in this research. Firstly, the ABCluster program (Zhang and Dolg, 2015) was performed to generate up to 120 000 initial isomer structures using the artificial bee algorithm (details in Sect. S1 of the Supplement). The universal force field (UFF) (Rappé et al., 1992) was chosen to select up to 1000 structures with lower energies from the initial isomer structures. Due to the inability of the UFF to effectively handle bond-breaking issues, we also utilized ion monomers for sampling during the configuration search of ternary clusters (Kubecka et al., 2019). From the most stable configuration of binary HIO_2–DMA clusters (Fig. S3 in the Supplement), it showed that the proton transfer from HIO_2 to DMA is forbidden in all clusters except for $(HIO_2)_1(DMA)_1$, indicating that it is difficult for this process to occur spontaneously. Hence, we only considered the ion monomers where HIO_3 donates protons or HIO_2/DMA accept protons. Secondly, 1000 structures for each cluster were pre-optimized by the PM7 semi-empirical method (Stewart, 2013) with the MOPAC 2016 program (Stewart, 2016) to choose 100 structures with relatively low energies. Then 100 structures were optimized at the ωB97X-D/6-31+G* (for H, C, N, and O atoms) and LANL2DZ (for I atom) levels of theory (Yang et al., 2009; Elm, 2013) to find 10 relatively stable structures among all of them. Finally, 10 stable structures were reoptimized at the ωB97X-D/6-311++G (3df, 3pd) (for H, C, N, and O atoms) and aug-cc-pVTZ-PP (for I atom) levels of theory (Frisch et al., 1984; Peterson, 2003; Chai and Head-Gordon, 2008; Elm and Kristensen, 2017) together with the calculations of vibrational frequencies. Notably, even though we try our best to search for the global minimum configurations of clusters considering the computational cost, saving 1000 local minima from the ABCluster search and selecting the lowest 100 cluster configurations based on PM7 may lead to the global minimum cluster being missed (Kurfman et al., 2021). Additionally, we manually constructed some potential stable clusters with multiple hydrogen and halogen bonding sites based on the chemical intuition. All quantum chemical calculations were performed using the Gaussian 09 package (Frisch et al., 2009) to identify the most stable conformations of each cluster.

Afterwards, the single-point energy correction was carried out by the RI-CC2/aug-cc-pVTZ (for H, C, N, and O atoms) and aug-cc-pVTZ-PP with ECP28MDF (for I atom) using the Turbomole program (Ahlrichs et al., 1989) because of the good agreement between simulated results (e.g., the cluster formation rates) at this theoretical level with the experimental results or field measurements through a random cancellation of errors (Almeida et al., 2013; Lu et al., 2020; Kürten et al., 2018). To assess the reliability of the RI-CC2 method, we compared the simulated cluster formation rates obtained at the ωB97X-D/6-311++G (3df, 3pd), RI-CC2/aug-cc-pVTZ, and DLPNO-CCSD(T)/aug-cc-pVTZ levels of theory with the CLOUD experiment results (He et al., 2021) (Fig. 1 and details can be found in Sect. S2 in the Supplement). As shown in Fig. 1, without performing single-point energy correction, the cluster formation rates simulated at the ωB97X-D/6-311++G (3df, 3pd) level of theory (the diamond points) are significantly lower than the experimental results (the circular points). Therefore, we chose to perform the single-point correction to obtain simulated cluster formation rates that agree more with the experimental results. Compared to the results of the DLPNO-CCSD(T) method, the simulated cluster formation rates based on the RI-CC2 method are more consistent with the experimental results at $T = 263$ K. Moreover, at $T = 283$ K, the RI-CC2 results are closer to lower cluster formation rates from the experiments and overestimate higher cluster formation rates from the experiments by less than 2 orders of magnitude. Considering that the results based on the RI-CC2 method agree the most with experimental results while saving computational resources, we finally chose the RI-CC2 method for single-point correction. It is important to note that this does not imply RI-CC2 results are inherently more accurate than those obtained using the DLPNO-CCSD(T) method. We cautiously state that the choice of the RI-CC2 method in this study is due to its ability to effectively match the experimental results through a random cancellation of errors (details can be found in Sect. S2) while saving computational resources.

In the present study, the Gibbs free energy of formation (ΔG, kcal mol^{-1}) of clusters was calculated as

$$\Delta G = \Delta E_{\mathrm{RI-CC2}} + \Delta G_{\mathrm{thermal}}^{\omega\mathrm{B97X-D}},$$

where $\Delta E_{\mathrm{RI-CC2}}$ is the electronic contribution obtained at the RI-CC2/aug-cc-pVTZ (for H, C, N, and O atoms) and aug-cc-pVTZ-PP with ECP28MDF (for I atom) levels of theory, and $\Delta G_{\mathrm{thermal}}^{\omega\mathrm{B97X-D}}$ is the thermal contribution calculated at the ωB97X-D/6-311++G (3df, 3pd) (for H, C, N, and O atoms) and aug-cc-pVTZ-PP with ECP28MDF (for I atom) levels of theory.

2.2 Atmospheric cluster dynamics code (ACDC) simulations

In order to investigate the effect of DMA on HIO_3–HIO_2 nucleation in marine areas, a series of ACDC simulations (McGrath et al., 2012) was performed under atmospheric conditions corresponding to mid-latitude coastal and high-latitude polar regions. By solving the birth–death equation, the ACDC simulations can obtain the cluster formation rates

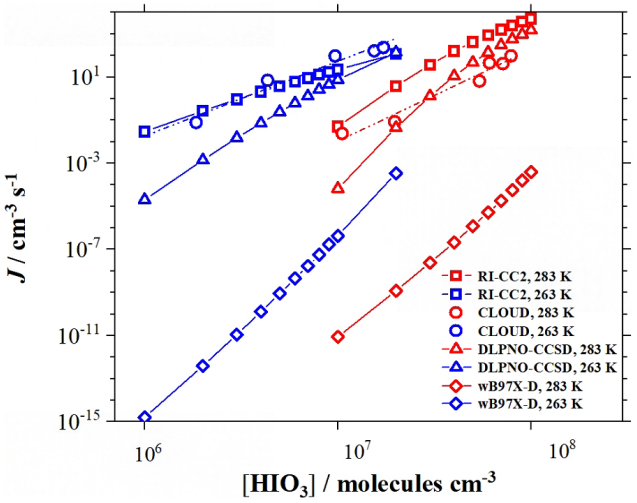

Figure 1. The cluster formation rates (J, $\mathrm{cm^{-3}\,s^{-1}}$) of the HIO_3–HIO_2 system obtained from experiment (CLOUD) and theoretical results at the RI-CC2 and DLPNO-CCSD levels of theory. The simulation was performed under the same conditions of an [HIO_3] of 10^6–10^8, an [HIO_2] of 2×10^4–2×10^6, $T = 283$ (red)/263 (blue) K, and a CS of $2.2\times10^{-3}\,\mathrm{s^{-1}}$. The circles represent the experimental results, the squares represent the theoretical results at RI-CC2/aug-cc-pVTZ (for H, C, N, and O atoms) and aug-cc-pVTZ-PP with ECP28MDF (for I atom) levels of theory, the triangles represent the theoretical results at the DLPNO-CCSD(T)/aug-cc-pVTZ (for H, C, N, and O atoms) and aug-cc-pVTZ-PP with ECP28MDF (for I atom) levels of theory, and the diamonds represent the theoretical results at the ωB97X-D/6-311++G (3df, 3pd) (for H, C, N, and O atoms) and aug-cc-pVTZ-PP with ECP28MDF (for I atom) levels of theory.

and formation pathways of clusters using the MATLAB program (Shampine and Reichelt, 1997). The birth–death equation can be written as follows:

$$\frac{\mathrm{d}c_i}{\mathrm{d}t} = \frac{1}{2}\sum_{j<i}\beta_{j,(i-j)}c_j c_{i-j} + \sum_j \gamma_{(i+j)\to i}c_{i+j} - \sum_j \beta_{i,j}c_i c_j - \frac{1}{2}\sum_{j<i}\gamma_{i\to j}c_i + Q_i - S_i,$$

where c_i is the concentration of cluster i, $\beta_{i,j}$ is the collision coefficient between cluster i and cluster j, $\gamma_{(i+j)\to i}$ is the evaporation coefficient of the cluster $(i+j)$ evaporating into cluster i and cluster j, Q_i is the external source term of cluster i, and S_i is the potential sink term for cluster i.

The collision coefficient $\beta_{i,j}$ can be written as

$$\beta_{i,j} = \left(\frac{3}{4\pi}\right)^{\frac{1}{6}}\left(\frac{6k_\mathrm{B}T}{m_i}+\frac{6k_\mathrm{B}T}{m_j}\right)^{\frac{1}{2}}\left(V_i^{\frac{1}{3}}+V_j^{\frac{1}{3}}\right)^2,$$

where k_B is the Boltzmann constant; T is the temperature; m_i is the mass of cluster i; and V_i is the van der Waals volume of cluster i, which is calculated by the improved marching tetrahedra (MT) approach (Lu and Chen, 2012b) using the Multiwfn 3.7 program.

The evaporation coefficient $\gamma_{(i+j)\to i}$ of the cluster was obtained from the collision coefficient and the specific balance between cluster formation via the collision and cluster loss via the evaporation:

$$\gamma_{(i+j)\to i} = \beta_{i,j}c_\mathrm{ref}\exp\left(\frac{\Delta G_{i+j}-\Delta G_i-\Delta G_j}{k_\mathrm{B}T}\right),$$

where c_ref is the monomer concentration under the reference pressure of 1 atm, and ΔG_i is the Gibbs free energy of the formation of cluster i.

The formation of clusters is accompanied by the competition between collision and evaporation. The clusters with a collision frequency higher than the total evaporation frequency ($\beta c/\Sigma\gamma > 1$) are considered to be stable from the perspective of nucleation kinetics. The detailed collision and total evaporation frequencies of the HIO_3–HIO_2–DMA system at all simulated temperatures and condensation sinks are listed in Tables S1–S4. The boundary conditions of the ACDC simulations are closely related to the ratio of the collision frequency between the clusters and monomer molecules at the concentration c to the total evaporation frequency of clusters. Moreover, the size of clusters in the simulation system also affects the accuracy of the simulation results (Fig. S1). We discuss the issues related to the size of clusters and the settings of boundary clusters in detail in Sect. S3 of the Supplement.

3 Results

3.1 Cluster stable configurations

The most stable configurations of the HIO_3–HIO_2–DMA ternary clusters at the ωB97X-D/6-311++G (3df, 3pd) (for H, C, N, and O atoms) and aug-cc-pVTZ-PP with ECP28MDF (for I atom) levels of theory are shown in Fig. 2. The structures of the HIO_2–DMA clusters can be found in Fig. S3 of the Supplement, and the Cartesian coordinates of all HIO_3–HIO_2–DMA and HIO_2–DMA clusters are shown in Table S7. The electrostatic potential (ESP) distribution (details in Sect. S4 of the Supplement) showed that the −NH group of DMA molecules can act as both donor and acceptor of non-covalent interactions. Hence, DMA can form stable ternary clusters through the space network formed by HBs and XBs. Moreover, acid-base proton transfer can be found in all ternary clusters except for the $(HIO_3)_1(HIO_2)_2(DMA)_1$ and $(HIO_3)_1(HIO_2)_3(DMA)_2$ clusters. It has been shown in previous studies on HIO_3–DMA and HIO_3–HIO_2 systems that acid-base proton transfer occurred between HIO_3 and HIO_2/DMA (Zhang et al., 2022a; Ning et al., 2022; Liu et al., 2023). The gas-phase basicity of DMA is strong ($896.5\,\mathrm{kJ\,mol^{-1}}$) (Yang et al., 2018). Hence, DMA is capable of efficiently stabilizing acidic precursors through acid-base interactions. Moreover, amphoteric HIO_2 molecules, the acid

dissociation constant (pK_a) which is 6.0 (Schmitz, 2008), can also exhibit base-like behavior in the neutral nucleation process of HIO_3–HIO_2 (Zhang et al., 2022a; Liu et al., 2023). This indicates that DMA may play a role similar to HIO_2 in the neutral nucleation process driven by HIO_3.

In order to assess the effect of DMA on the proton transfer process, the analysis of the proton transfer was performed based on the change in bond length at corresponding positions that conduct acid-base reaction. The number of proton transfers between different precursors in ternary clusters and the total number of proton transfers are summarized in Table S8. As shown in Table S8, among most of the ternary clusters, HIO_3 will preferentially interact with DMA, which possesses strong basicity, in the process of proton transfer. Afterwards, the remaining HIO_3 can perform proton transfer with the amphoteric HIO_2, which can also exhibit base-like behavior under this circumstance. It is worth noting that, in terms of the stability (evaluated by ΔG) of clusters, the proton transfer plays a crucial role. Taking two three-molecule clusters, $(HIO_3)_2(HIO_2)_1$ ($\Delta G = -30.05\,kcal\,mol^{-1}$) and $(HIO_3)_1(HIO_2)_1(DMA)_1$ ($\Delta G = -35.19\,kcal\,mol^{-1}$), as an example, we observed that the $(HIO_3)_2(HIO_2)_1$ cluster with higher energy is formed through three XBs and one HB, while the $(HIO_3)_1(HIO_2)_1(DMA)_1$ cluster with lower energy is formed through three HBs after proton transfer. Additionally, when the number of proton transfers is the same, clusters with more halogen bonds formed by HIO_2 generally have lower ΔG, which can be seen from $(HIO_3)_1(HIO_2)_2(DMA)_1$ ($\Delta G = -50.07\,kcal\,mol^{-1}$, formed by three XBs and two HBs) and $(HIO_2)_4$ ($\Delta G = -58.08\,kcal\,mol^{-1}$, formed by four XBs) clusters. Similar results can also be observed in other ternary clusters. As for the water (H_2O) molecules, they are indispensable in the formation process of marine aerosols. However, previous studies have indicated that H_2O contributes less significantly to strong acid-base systems dominated by proton transfer, such as the H_2SO_4–DMA system (Kürten et al., 2018; Olenius et al., 2017; Liu et al., 2021b). The HIO_3–HIO_2–DMA system exhibits a clustering pattern similar to the H_2SO_4–DMA system, with proton transfer processes in almost all ternary clusters. Hence, we speculate that the contribution of H_2O to the HIO_3–HIO_2–DMA system is relatively weak, similar to the contribution of H_2O to the H_2SO_4–DMA system. In addition, considering that the introduction of hydrated clusters requires a large amount of additional quantum chemical calculations, which are time-consuming in the current workflow, the impact of H_2O is not considered in the present study.

In summary, the structural analysis shows that DMA can form stable clusters with iodine oxoacids via HBs, XBs and proton transfer, laying the foundation for promoting HIO_3–HIO_2 nucleation. Moreover, DMA can preferentially accept the proton from HIO_3 in the most stable configurations of HIO_3–HIO_2–DMA clusters, while the amphoteric HIO_2 can also exhibit similar behavior.

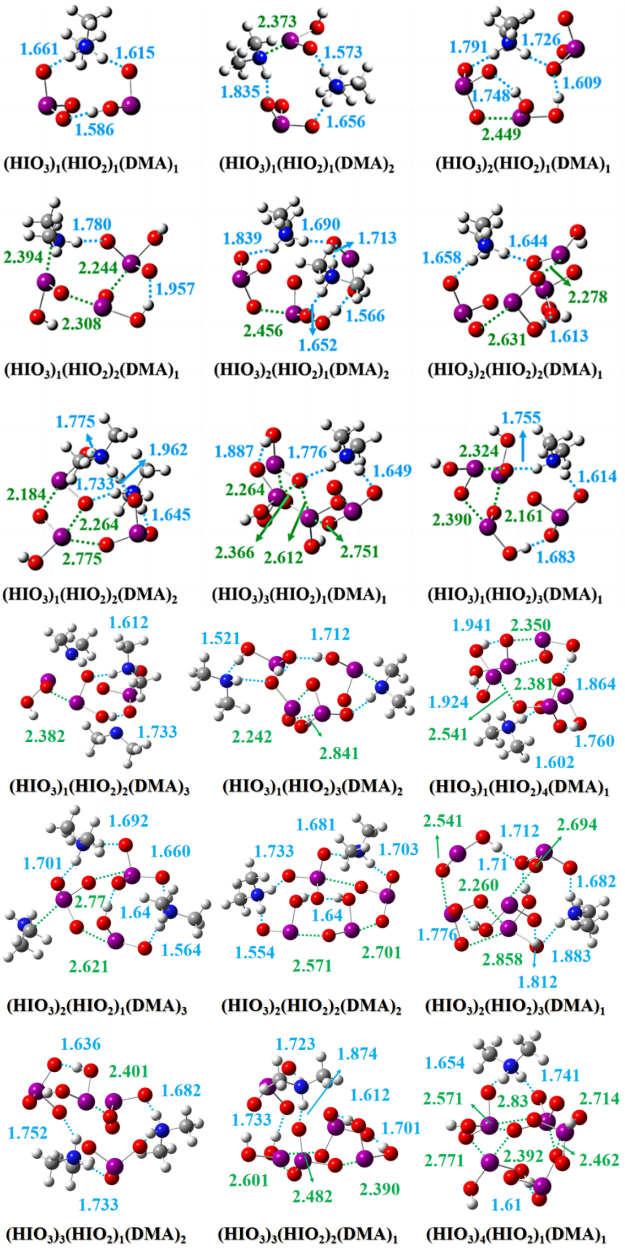

Figure 2. The most stable structures of HIO_3–HIO_2–DMA clusters identified at the ωB97X-D/6-311++G (3df, 3pd) (for H, C, N, and O atoms) and aug-cc-pVTZ-PP with ECP28MDF (for I atom) levels of theory. The white, grey, blue, red, and purple balls represent the H, C, N, O, and I atoms, respectively. The hydrogen bonds and halogen bonds are shown in dashed blue and green lines, respectively. The values of bond lengths are given in Å.

3.2 Cluster formation pathways

To further study the kinetic behavior of DMA in the nucleation process, the ACDC was used to simulate the nucleation pathways under marine atmospheric conditions. Firstly, a specific simulation was performed under atmospheric conditions reported in Zhejiang, an intersection of high-[DMA]-

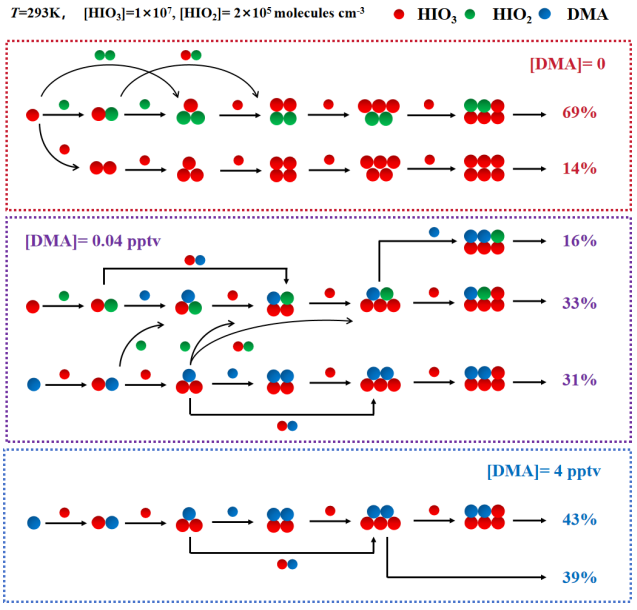

Figure 3. The cluster formation pathways and the contribution of main pathways to the total cluster formation rates under field conditions of Zhejiang at an $[HIO_3]$ of 1.0×10^7 molecules cm^{-3}; an $[HIO_2]$ of 2.0×10^5 molecules cm^{-3}; a [DMA] of 0 (red), 0.04 (purple), and 4 (blue) pptv; $T = 293$ K; and a CS of 1.0×10^{-2} s^{-1}. The red, green, and blue balls represent the HIO_3, HIO_2, and DMA molecules, respectively.

pollution air masses and marine iodine air masses on the east coast of China (Zhu et al., 2019; Zhang et al., 2023). The main cluster formation pathways, which contribute more than 5 % to the total cluster formation rates, at an $[HIO_3]$ of 1.0×10^7 molecules cm^{-3}, an $[HIO_2]$ of 2.0×10^5 molecules cm^{-3}, and $T = 293$ K, are shown in Fig. 3. The average condensation sink (CS) was estimated and set to be 1.0×10^{-2} s^{-1} for polluted coastal regions (Ning et al., 2022). In Fig. 3, we present the simulation results under three different [DMA] conditions ([DMA] of 0, 0.04, and 4 pptv) to evaluate the influence of DMA on the nucleation process of iodine oxoacids. As shown in Fig. 3, with the increase in [DMA], the cluster formation pathways in the simulated system undergo continuous changes. The primary pathway shifts from the binary HIO_3–HIO_2 pathway to the ternary HIO_3–HIO_2–DMA pathway and further to the binary HIO_3–DMA pathway. Hence, DMA might be involved in the nucleation process of the HIO_3–HIO_2 system in coastal regions, especially in regions affected by high [DMA].

The simulated nucleation pathway under this specific condition has proved the participation of DMA in HIO_3–HIO_2 nucleation. However, since HIO_x ($x = 2, 3$) and DMA originate from different sources, the concentrations of precursors should be changed to better represent the situation of regions with different iodine and amine emission intensities. Therefore, to further study the involvement of DMA in nucleation pathways under various oceanic atmospheric conditions, the contributions of the main cluster formation pathways at different concentrations are simulated, and the results are shown in Fig. 4. It is worth noting that the concentration of HIO_2 changes together with that of HIO_3 from low to high since HIO_2 and HIO_3 are homologous iodine species. The ratio of $[HIO_3]$ to $[HIO_2]$ is about 20 to 100 depending on the concentration of iodine vapor (Yu et al., 2019; Baccarini et al., 2020; Rong et al., 2020; Xia et al., 2020; He et al., 2021; Sipilä et al., 2016). The ratio used in Fig. 4 is 50 according to the former field observations in Mace Head (Sipilä et al., 2016), and the other results obtained from two different ratios (20 and 100) of $[HIO_3]$ and $[HIO_2]$ can be seen from Sect. S5 of the Supplement.

As can be seen from Fig. 4, the contribution of DMA to the nucleation increases, with [DMA] rising from 10^{-3} to 1 pptv, and the dominating mechanism varies similarly to Fig. 3 from HIO_3–HIO_2 nucleation to HIO_3–HIO_2–DMA nucleation and then to HIO_3–DMA nucleation. Moreover, combining Figs. S4 and S5, an opposite trend in the dominant mechanism becomes apparent with the increase in $[HIO_2]$. Specifically, the primary nucleation mechanism shifts from HIO_3–DMA to HIO_3–HIO_2–DMA or from HIO_3–HIO_2–DMA to HIO_3–HIO_2 as $[HIO_2]$ increases. Notably, the HIO_3–HIO_2–DMA ternary mechanism is more significant when $[HIO_2]$ and [DMA] are similar. In contrast, when DMA (HIO_2) is much more abundant than HIO_2 (DMA), the pathways are overwhelmingly dominated by rapid binary nucleation involving HIO_3 and DMA (HIO_2) with higher concentration. This phenomenon may be attributed to the similar stabilizing effects of DMA and HIO_2 on HIO_3 nucleation, where the component with a higher concentration plays a more significant role. Consequently, the component with a lower concentration exerts less influence, primarily due to the limited availability of HIO_3. This indicates that when [DMA] reaches 10^{-1} to 1 pptv, the proportion of DMA-containing pathways will approach 100 % (Fig. 4), indicating significant involvement of DMA on the HIO_3–HIO_2 system. As mentioned in the Introduction, marine regions are not lacking in high-intensity sources of DMA, especially in polluted coastal areas. However, currently reported experiments and model simulations have not yet focused on the ternary HIO_3–HIO_2–DMA mechanism. Therefore, in the next section, we evaluate the nucleation ability of the newly proposed HIO_3–HIO_2–DMA mechanism through comparison with classical nucleation mechanisms or observation results to comprehensively assess the environmental significance of the HIO_3–HIO_2–DMA mechanism in the broad marine regions.

3.3 Cluster formation rates

The cluster formation pathway showed that DMA may significantly participate in HIO_3–HIO_2 nucleation. However, the influence of DMA on the cluster formation rates (J, cm^{-3} s^{-1}) of the HIO_3–HIO_2 nucleation is still unknown. To evaluate the influence of DMA on the HIO_3–HIO_2

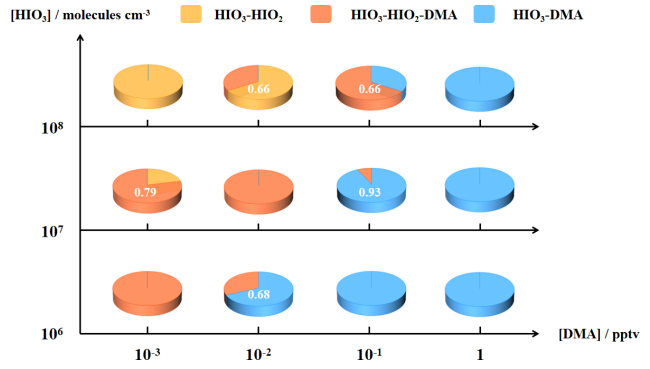

Figure 4. The contribution of main nucleation pathways at different concentrations of precursors, with an [HIO_3] of 10^6–10^8 molecules cm^{-3}, an [HIO_2] of 2.0×10^4–2.0×10^6 molecules cm^{-3}, and a [DMA] of 10^{-3}–1 pptv. The simulated temperature and condensation sink are 283 K and 2.0×10^{-3} s^{-1} as typical values for oceanic atmosphere. The proportions of the contribution of HIO_3–HIO_2, HIO_3–HIO_2–DMA, and HIO_3–DMA are shown in yellow, orange, and blue, respectively.

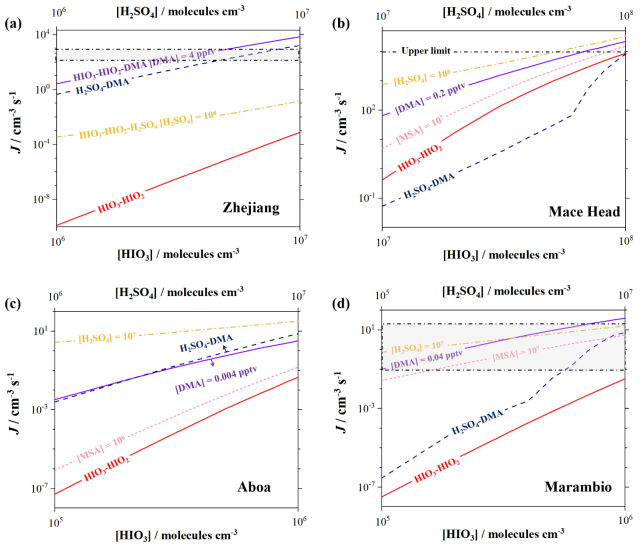

Figure 5. The cluster formation rates (J, cm^{-3} s^{-1}) of the HIO_3–HIO_2 (red), HIO_3–HIO_2–DMA (purple), HIO_3–HIO_2–H_2SO_4 (yellow), HIO_3–HIO_2–MSA (pink), and H_2SO_4–DMA (blue) systems under the simulated conditions of **(a)** Zhejiang, with an [HIO_3] of 10^6–10^7, an [HIO_2] of 2×10^4–2×10^5, an [H_2SO_4] of 10^6–10^8 molecules cm^{-3}, and a [DMA] of 4 pptv; **(b)** Mace Head, with an [HIO_3] of 10^7–10^8, an [HIO_2] of 2×10^5–2×10^6, an [H_2SO_4] of 10^7–10^8, an [MSA] of 10^7 molecules cm^{-3}, and a [DMA] of 0.2 pptv; **(c)** Aboa, with an [HIO_3] of 10^5–10^6, an [HIO_2] of 2×10^3–2×10^4, an [H_2SO_4] of 10^6–10^7, an [MSA] of 10^6 molecules cm^{-3}, and a [DMA] of 0.004 pptv; and **(d)** Marambio, with an [HIO_3] of 10^5–10^6, an [HIO_2] of 2×10^3–2×10^4, an [H_2SO_4] of 10^5–10^7, an [MSA] of 10^7 molecules cm^{-3}, and a [DMA] of 0.04 pptv. The shaded area (grey) represents the actual nucleation rates observed locally.

system and the environmental significance of the HIO_3–HIO_2–DMA system, we compared the J of the HIO_3–HIO_2 (red), HIO_3–HIO_2–DMA (purple), HIO_3–HIO_2–H_2SO_4 (yellow), HIO_3–HIO_2–MSA (pink), and H_2SO_4–DMA (blue) systems under the simulated conditions of typical marine and polar regions. The results of the HIO_3–HIO_2–H_2SO_4 (Zu et al., 2024) and HIO_3–HIO_2–MSA systems (https://doi.org/10.5194/egusphere-2023-2084) were obtained from former studies at the same level of theory as the HIO_3–HIO_2–DMA system. The configurations of H_2SO_4–DMA clusters were obtained from the Atmospheric Cluster Database (ACDB) (Elm, 2019). Subsequently, geometric optimizations and frequency calculations were performed at the same (ωB97X-D/6-311++G (3df, 3pd)) level of theory as the HIO_3–HIO_2–DMA system. Notably, we believe that the influence of other mechanisms (e.g., HIO_3–HIO_2–A) is widespread and significant. However, due to the lack of available data, other mechanisms are not discussed in this study and will be considered in further studies.

The Zhejiang region experiences frequent NPF events, closely associated with a high-intensity iodine-driven nucleation process (Yu et al., 2019). However, our simulation results under the conditions of Zhejiang (Xia et al., 2020; Yu et al., 2019) indicate that relying solely on HIO_3–HIO_2 nucleation (red curve in Fig. 5a) appears insufficient to explain the rapid formation rates of an ambient environment (grey-shaded area). It is noteworthy that the NPF events in the local area is found to be influenced not only by marine components but also by urban pollutants (Zhu et al., 2019; Liu et al., 2022). During polluted periods, the emission capacity of gas-phase DMA is exceptionally strong, and high concentrations of DMA can further enhance the J of HIO_3–HIO_2, resulting in a significant enhancement of up to 10^8 at a [DMA] of 4 pptv. Notably, the increase in the concentrations of HIO_2 and DMA can both enhance the J to match the field observations, indicating that HIO_2 and DMA molecules exhibit a synergistic effect on HIO_3 nucleation, which may have significant contributions to NPF events in the polluted coastal areas where marine iodine species intersect with high concentrations of DMA. Moreover, the urban pollution also leads to an abundant concentration of gas-phase H_2SO_4. This renders the impact of the HIO_3–HIO_2–H_2SO_4 and H_2SO_4–DMA mechanisms non-negligible. As shown in Fig. 5a, the simulated J of the H_2SO_4–DMA and HIO_3–HIO_2–H_2SO_4 systems (dashed blue line) is about 1 or 4 orders of magnitude lower than that of the HIO_3–HIO_2–DMA system, respectively. This indirectly indicates that the HIO_3–HIO_2 system promoted by DMA possesses remarkable nucleation ability and might make unexpected contributions in specific regions, thereby providing an explanation for some missing fluxes of particles in the atmosphere.

In contrast, the results from the Mace Head region present a different situation. Previous studies have demonstrated that

local nucleation is primarily driven by high concentrations of HIO_3 (Sipilä et al., 2016). The simulated results showed that the J of the HIO_3–HIO_2 system can reach up to levels of $10^4\,cm^{-3}\,s^{-1}$, which is consistent with the upper limit of formation rates reported in the field observation (Sipilä et al., 2016). Furthermore, we evaluated the potential impact of DMA and other precursors on the J of the HIO_3–HIO_2 system based on the concentrations from model simulations or gas-phase measurements reported at Mace Head (Yu and Luo, 2014; Sipilä et al., 2016). The results indicate that DMA can promote the J significantly only at lower iodine concentrations. As iodine oxoacids increase, the J of the HIO_3–HIO_2–DMA system gradually approaches that of the HIO_3–HIO_2 system, indicating a less significant enhancement by DMA. Similar patterns regarding the enhancement by H_2SO_4 and MSA can also be shown. This indicates that in primitive regions with abundant iodine sources, even if the precursors (DMA, H_2SO_4, and MSA) can reach the high concentrations used in the simulation in this study, their corresponding enhancement is limited. The primary nucleation mechanism is likely to be the HIO_3–HIO_2 mechanism, which is supported by the on-site measurements of the components of nanoparticles (Sipilä et al., 2016).

Recent research has shown that the ice-influenced ocean may also be important sources of DMA (Dall'Osto et al., 2017, 2019). Hence, we also evaluate the environmental significance of the HIO_3–HIO_2–DMA system in the ice-covered polar regions. As shown in Fig. 5c, we performed a simulation under the conditions the Aboa station. The simulation results indicate that HIO_3–HIO_2–H_2SO_4 and H_2SO_4–DMA are more efficient nucleation mechanisms than the HIO_3–HIO_2–DMA system in the local area. Moreover, the simulated J of the HIO_3–HIO_2–DMA system is also slightly lower than the formation rates ($0.05–0.12\,cm^{-3}\,s^{-1}$) of the ion-induced H_2SO_4–A system reported by field observations (Jokinen et al., 2018). Hence, due to the overall lower concentrations of iodine and amine components, the nucleation process is predominantly driven by H_2SO_4 molecules. This suggests that in regions with scarce iodine and amine sources, the contribution of the DMA-enhanced HIO_3–HIO_2 mechanism to the particle formation is limited. In contrast, in the Marambio region with relatively abundant DMA and scarce iodine oxoacids (Quéléver et al., 2022; Wang et al., 2023), the HIO_3–HIO_2–DMA system may also have significant contributions (Fig. 5d). The [HIO_3] used in the simulation is still about an order of magnitude lower than [H_2SO_4] and [MSA]. However, [DMA] is about an order of magnitude higher than in the Aboa region. In this case, the J of the HIO_3–HIO_2 system is significantly enhanced by more than 10^3-fold by the relatively abundant DMA. Compared to the acidic components such as H_2SO_4 and MSA, DMA elevates the J of the HIO_3–HIO_2 system to the range of 10^{-1} to $10^1\,cm^{-3}\,s^{-1}$, matching the field observation results, while [DMA] is only $\frac{1}{10}$ of [H_2SO_4] and [MSA]. This indicates that, considering nucleation ability, the enhancement effect of DMA on the HIO_3–HIO_2 system may be superior to H_2SO_4 and MSA, which we speculate is likely related to the base stabilization effect of DMA within acidic clusters. Additionally, our results demonstrate that the nucleation ability of HIO_3–HIO_2–DMA is stronger than that of H_2SO_4–DMA. This means that the HIO_3–HIO_2–DMA ternary mechanism may be an important contributor to iodine-containing particles, especially in regions where there are sufficient iodine and amine sources.

In summary, the results show that the HIO_3–HIO_2–DMA ternary nucleation mechanism may have significant contributions to the formation of nanoparticles, especially in regions with abundant iodine and amine sources. This previously overlooked mechanism may provide an explanation for some missing fluxes of atmospheric iodine particles. Moreover, the observed formation rates in the field can result from multiple rapid-nucleation systems or may be solely attributed to a specific system, depending significantly on the variations in precursor concentrations in different regions. The nucleation process in the real atmosphere is complex. Hence, the simulation of scenarios where various components participate simultaneously is needed in the future study to accurately assess the roles of different components such as H_2SO_4, MSA, A, and DMA in the iodine oxoacid nucleation. This may contribute to a fundamental understanding of atmospheric particle formation, providing comprehensive insight into the entire evolution process of atmospheric aerosols.

4 Atmospheric significance and conclusion

The present study investigated iodine oxoacid nucleation enhanced by DMA under broad oceanic atmospheric conditions through quantum chemical calculations combined with ACDC simulations. As a basic precursor to stabilize acid, DMA can form the stable ternary clusters with HIO_3 and HIO_2, in which DMA can preferentially accept the proton from HIO_3. Kinetically, the participation of DMA in the cluster formation pathways of the iodine oxoacid system is significant at the 10^{-1} to 1 pptv level of [DMA]. Furthermore, DMA can enhance the cluster formation rates of the HIO_3–HIO_2 system in marine and polar regions near DMA sources by more than 10^3-fold. Compared to the classical nucleation mechanism, the HIO_3–HIO_2–DMA mechanism exhibits strong nucleation ability, worthy of consideration as a promising mechanism in marine and polar regions rich in amine sources. The nucleation mechanism in the real atmosphere is more complex and may result from multiple rapid-nucleation systems, depending significantly on the variations in precursor concentrations in different regions. Hence, there is an urgent need for the development of atmospheric models that comprehensively consider the coupling effects of multiple mechanisms.

Data availability. The data in this article can be made available from the corresponding authors upon request (Ling Liu: lingliu@bit.edu.cn and Xiuhui Zhang: zhangxiuhui@bit.edu.cn).

Supplement. The supplement related to this article is available online at: https://doi.org/10.5194/acp-24-5823-2024-supplement.

Author contributions. XZ designed and supervised the research. HZ performed the quantum chemical calculations and the ACDC simulations. HZ and LL analyzed data. HZ, LL, and XZ wrote the paper. XZ, LL, BC, and YL reviewed and edited the paper. All authors commented on the paper.

Competing interests. The contact author has declared that none of the authors has any competing interests.

Disclaimer. Publisher's note: Copernicus Publications remains neutral with regard to jurisdictional claims made in the text, published maps, institutional affiliations, or any other geographical representation in this paper. While Copernicus Publications makes every effort to include appropriate place names, the final responsibility lies with the authors.

Acknowledgements. We acknowledge the National Supercomputing Center in Shenzhen for providing the computational resources and the Turbomole program.

Financial support. This research has been supported by the National Science Fund for Distinguished Young Scholars (grant no. 22225607) and the National Natural Science Foundation of China (grant nos. 42105101, 22376013, 22122610, and 21976015).

Review statement. This paper was edited by Tuukka Petäjä and reviewed by Jonas Elm and one anonymous referee.

References

Ahlrichs, R., Bar, M., Horn, H., and Kolmel, C.: Electronic-structure calculations on workstation computers – the program system turbomole, Chem. Phys. Lett., 162, 165–169, https://doi.org/10.1016/0009-2614(89)85118-8, 1989.

Almeida, J., Schobesberger, S., Kürten, A., Ortega, I. K., Kupiainen-Määttä, O., Praplan, A. P., Adamov, A., Amorim, A., Bianchi, F., Breitenlechner, M., David, A., Dommen, J., Donahue, N. M., Downard, A., Dunne, E., Duplissy, J., Ehrhart, S., Flagan, R. C., Franchin, A., Guida, R., Hakala, J., Hansel, A., Heinritzi, M., Henschel, H., Jokinen, T., Junninen, H., Kajos, M., Kangasluoma, J., Keskinen, H., Kupc, A., Kurtén, T., Kvashin, A. N., Laaksonen, A., Lehtipalo, K., Leiminger, M., Leppa, J., Loukonen, V., Makhmutov, V., Mathot, S., McGrath, M. J., Nieminen, T., Olenius, T., Onnela, A., Petäjä, T., Riccobono, F., Riipinen, I., Rissanen, M., Rondo, L., Ruuskanen, T., Santos, F. D., Sarnela, N., Schallhart, S., Schnitzhofer, R., Seinfeld, J. H., Simon, M., Sipilä, M., Stozhkov, Y., Stratmann, F., Tomé, A., Tröstl, J., Tsagkogeorgas, G., Vaattovaara, P., Viisanen, Y., Virtanen, A., Vrtala, A., Wagner, P. E., Weingartner, E., Wex, H., Williamson, C., Wimmer, D., Ye, P. L., Yli-Juuti, T., Carslaw, K. S., Kulmala, M., Curtius, J., Baltensperger, U., Worsnop, D. R., Vehkamäki, H., and Kirkby, J.: Molecular understanding of sulphuric acid-amine particle nucleation in the atmosphere, Nature, 502, 359–363, https://doi.org/10.1038/nature12663, 2013.

Baccarini, A., Karlsson, L., Dommen, J., Duplessis, P., Vüllers, J., Brooks, I. M., Saiz-Lopez, A., Salter, M., Tjernström, M., Baltensperger, U., Zieger, P., and Schmale, J.: Frequent new particle formation over the high Arctic pack ice by enhanced iodine emissions, Nat. Commun., 11, 4924, https://doi.org/10.1038/s41467-020-18551-0, 2020.

Chai, J.-D. and Head-Gordon, M.: Long-range corrected hybrid density functionals with damped atom–atom dispersion corrections, Phys. Chem. Chem. Phys., 10, 6615–6620, https://doi.org/10.1039/B810189B, 2008.

Chen, D. P., Li, D. F., Wang, C. W., Liu, F. Y., and Wang, W. L.: Formation mechanism of methanesulfonic acid and ammonia clusters: A kinetics simulation study, Atmos. Environ., 222, 117161, https://doi.org/10.1016/j.atmosenv.2019.117161, 2020a.

Chen, D. P., Li, D. F., Wang, C. W., Luo, Y., Liu, F. Y., and Wang, W. L.: Atmospheric implications of hydration on the formation of methanesulfonic acid and methylamine clusters: A theoretical study, Chemosphere, 244, 125538, https://doi.org/10.1016/j.chemosphere.2019.125538, 2020b.

Chen, D., Shen, Y., Wang, J., Gao, Y., Gao, H., and Yao, X.: Mapping gaseous dimethylamine, trimethylamine, ammonia, and their particulate counterparts in marine atmospheres of China's marginal seas – Part 1: Differentiating marine emission from continental transport, Atmos. Chem. Phys., 21, 16413–16425, https://doi.org/10.5194/acp-21-16413-2021, 2021.

Corral, A. F., Choi, Y., Collister, B. L., Crosbie, E., Dadashazar, H., DiGangi, J. P., Diskin, G. S., Fenn, M., Kirschler, S., and Moore, R. H. J. E. S. A.: Dimethylamine in cloud water: a case study over the northwest Atlantic Ocean, Environ. Sci.-Atmos., 2, 1534–1550, https://doi.org/10.1039/D2EA00117A, 2022.

Dall'Osto, M., Beddows, D. C. S., Tunved, P., Krejci, R., Ström, J., Hansson, H. C., Yoon, Y. J., Park, K. T., Becagli, S., Udisti, R., Onasch, T., O'Dowd, C. D., Simo, R., and Harrison, R. M.: Arctic sea ice melt leads to atmospheric new particle formation, Sci. Rep., 7, 3318, https://doi.org/10.1038/s41598-017-03328-1, 2017.

Dall'Osto, M., Airs, R. L., Beale, R., Cree, C., Fitzsimons, M. F., Beddows, D., Harrison, R. M., Ceburnis, D., O'Dowd, C., Rinaldi, M., Paglione, M., Nenes, A., Decesari, S., and Simó, R.: Simultaneous Detection of Alkylamines in the Surface Ocean and Atmosphere of the Antarctic Sympagic Environment, Acs Earth Space Chem., 3, 854–862, https://doi.org/10.1021/acsearthspacechem.9b00028, 2019.

Ehn, M., Vuollekoski, H., Petäjä, T., Kerminen, V. M., Vana, M., Aalto, P., de Leeuw, G., Ceburnis, D., Dupuy, R., O'Dowd, C. D., and Kulmala, M.: Growth rates during coastal and marine new particle formation in western Ireland, J. Geophys. Res.-Atmos., 115, D18218, https://doi.org/10.1029/2010jd014292, 2010.

Elm, J.: Assessment of binding energies of atmospherically relevant clusters, Phys. Chem. Chem. Phys. 15, 16442–16445, https://doi.org/10.1039/C3CP52616J, 2013.

Elm, J.: An Atmospheric Cluster Database Consisting of Sulfuric Acid, Bases, Organics, and Water, Acs Omega, 4, 10965–10974, https://doi.org/10.1021/acsomega.9b00860, 2019.

Elm, J.: Clusteromics I: Principles, Protocols, and Applications to Sulfuric Acid-Base Cluster Formation, Acs Omega, 6, 7804–7814, https://doi.org/10.1021/acsomega.1c00306, 2021a.

Elm, J.: Clusteromics II: Methanesulfonic Acid-Base Cluster Formation, Acs Omega, 6, 17035–17044, https://doi.org/10.1021/acsomega.1c02115, 2021b.

Elm, J. and Kristensen, K.: Basis set convergence of the binding energies of strongly hydrogen-bonded atmospheric clusters, Phys. Chem. Chem. Phys., 19, 1122–1133, https://doi.org/10.1039/c6cp06851k, 2017.

Elm, J., Passananti, M., Kurtén, T., and Vehkamäki, H.: Diamines Can Initiate New Particle Formation in the Atmosphere, J. Phys. Chem. A, 121, 6155–6164, https://doi.org/10.1021/acs.jpca.7b05658, 2017.

Facchini, M. C., Decesari, S., Rinaldi, M., Carbone, C., Finessi, E., Mircea, M., Fuzzi, S., Moretti, F., Tagliavini, E., Ceburnis, D., and O'Dowd, C. D.: Important Source of Marine Secondary Organic Aerosol from Biogenic Amines, Environ. Sci. Technol., 42, 9116–9121, https://doi.org/10.1021/es8018385, 2008.

Frisch, M. J., Pople, J. A., and Binkley, J. S.: Self-consistent molecular orbital methods 25. Supplementary functions for Gaussian basis sets, J. Chem. Phys., 80, 3265–3269, https://doi.org/10.1063/1.447079, 1984.

Frisch, M. J., Trucks, G. W., Schlegel, H. B., Scuseria, G. E., Robb, M. A., Cheeseman, J. R., Scalmani, G., Barone, V., Mennucci, B., Petersson, G.A., Nakatsuji, H., Caricato, M., Li, X., Hratchian, H. P., Izmaylov, A. F., Bloino, J., Zheng, G., Sonnenberg, J. L., Hada, M., E., M., Toyota, K., Fukuda, R., Hasegawa, J., Ishida, M., Nakajima, T., Honda, Y., Kitao, O., Nakai, H., Vreven, T., Montgomery, J. A., Peralta, J. E., Ogliaro, F., Bearpark, M., Heyd, J. J., Brothers, E., Kudin, K. N., Staroverov, V. N., Kobayashi, R., Normand, J., Raghavachari, K., Rendell, A., Burant, J. C., Iyengar, S. S., Tomasi, J., Cossi, M., Rega, N., Millam, J. M., Klene, M., Knox, J. E., Cross, J. B., Bakken, V., Adamo, C., Jaramillo, J., Gomperts, R., Stratmann, R. E., Yazyev, O., Austin, A. J., Cammi, R., Pomelli, C., Ochterski, J. W., Martin, R. L., Morokuma, K., Zakrzewski, V. G., Voth, G. A., Salvador, P., Dannenberg, J. J., Dapprich, S., Daniels, A. D., Farkas, O., Foresman, J. B., Ortiz, J. V., Cioslowski, J., and Fox, D. J.: Gaussian 09, Revision A.1. Gaussian Inc, Wallingford CT., Gaussian 09, Revision A.1. Gaussian Inc, Wallingford CT, https://gaussian.com/g09citation/ (last access: 12 May 2024), 2009.

Gibb, S. W., Mantoura, R. F. C., and Liss, P. S.: Ocean-atmosphere exchange and atmospheric speciation of ammonia and methylamines in the region of the NW Arabian Sea, Global Biogeochem. Cy., 13, 161–177, https://doi.org/10.1029/98gb00743, 1999.

Gong, J., Zhu, T., Kipen, H., Wang, G., Hu, M., Guo, Q., Ohman-Strickland, P., Lu, S. E., Wang, Y., Zhu, P., Rich, D. Q., Huang, W., and Zhang, J.: Comparisons of ultrafine and fine particles in their associations with biomarkers reflecting physiological pathways, Environ. Sci. Technol., 48, 5264–5273, https://doi.org/10.1021/es5006016, 2014.

Gronberg, L., Lovkvist, P., and Jonsson, J. A.: Measurement of aliphatic amines in ambient air and rainwater, Chemosphere, 24, 1533–1540, https://doi.org/10.1016/0045-6535(92)90273-t, 1992.

Haywood, J. and Boucher, O.: Estimates of the direct and indirect radiative forcing due to tropospheric aerosols: A review, Rev. Geophys., 38, 513–543, https://doi.org/10.1029/1999rg000078, 2000.

He, X. C., Tham, Y. J., Dada, L., Wang, M. Y., Finkenzeller, H., Stolzenburg, D., Iyer, S., Simon, M., Kurten, A., Shen, J. L., Rorup, B., Rissanen, M., Schobesberger, S., Baalbaki, R., Wang, D. S., Koenig, T. K., Jokinen, T., Sarnela, N., Beck, L. J., Almeida, J., Amanatidis, S., Amorim, A., Ataei, F., Baccarini, A., Bertozzi, B., Bianchi, F., Brilke, S., Caudillo, L., Chen, D. X., Chiu, R., Chu, B. W., Dias, A., Ding, A. J., Dommen, J., Duplissy, J., El Haddad, I., Carracedo, L. G., Granzin, M., Hansel, A., Heinritzi, M., Hofbauer, V., Junninen, H., Kangasluoma, J., Kemppainen, D., Kim, C., Kong, W. M., Krechmer, J. E., Kvashin, A., Laitinen, T., Lamkaddam, H., Lee, C. P., Lehtipalo, K., Leiminger, M., Li, Z. J., Makhmutov, V., Manninen, H. E., Marie, G., Marten, R., Mathot, S., Mauldin, R. L., Mentler, B., Mohler, O., Muller, T., Nie, W., Onnela, A., Petaja, T., Pfeifer, J., Philippov, M., Ranjithkumar, A., Saiz-Lopez, A., Salma, I., Scholz, W., Schuchmann, S., Schulze, B., Steiner, G., Stozhkov, Y., Tauber, C., Tome, A., Thakur, R. C., Vaisanen, O., Vazquez-Pufleau, M., Wagner, A. C., Wang, Y. H., Weber, S. K., Winkler, P. M., Wu, Y. S., Xiao, M., Yan, C., Ye, Q., Ylisirnio, A., Zauner-Wieczorek, M., Zha, Q. Z., Zhou, P. T., Flagan, R. C., Curtius, J., Baltensperger, U., Kulmala, M., Kerminen, V. M., Kurten, T., Donahue, N. M., Volkamer, R., Kirkby, J., Worsnop, D. R., and Sipila, M.: Role of iodine oxoacids in atmospheric aerosol nucleation, Science, 371, 589-595, https://doi.org/10.1126/science.abe0298, 2021.

He, X.-C., Simon, M., Iyer, S., Xie, H.-B., Rörup, B., Shen, J., Finkenzeller, H., Stolzenburg, D., Zhang, R., Baccarini, A., Tham, Y. J., Wang, M., Amanatidis, S., Piedehierro, A. A., Amorim, A., Baalbaki, R., Brasseur, Z., Caudillo, L., Chu, B., Dada, L., Duplissy, J., El Haddad, I., Flagan, R. C., Granzin, M., Hansel, A., Heinritzi, M., Hofbauer, V., Jokinen, T., Kemppainen, D., Kong, W., Krechmer, J., Kürten, A., Lamkaddam, H., Lopez, B., Ma, F., Mahfouz, N. G. A., Makhmutov, V., Manninen, H. E., Marie, G., Marten, R., Massabò, D., Mauldin, R. L., Mentler, B., Onnela, A., Petäjä, T., Pfeifer, J., Philippov, M., Ranjithkumar, A., Rissanen, M. P., Schobesberger, S., Scholz, W., Schulze, B., Surdu, M., Thakur, R. C., Tomé, A., Wagner, A. C., Wang, D., Wang, Y., Weber, S. K., Welti, A., Winkler, P. M., Zauner-Wieczorek, M., Baltensperger, U., Curtius, J., Kurtén, T., Worsnop, D. R., Volkamer, R., Lehtipalo, K., Kirkby, J., Donahue, N. M., Sipilä, M., and Kulmala, M.: Iodine oxoacids enhance nucleation of sulfuric acid particles in the atmosphere, Science, 382, 1308–1314, https://doi.org/10.1126/science.adh2526, 2023.

Hoffmann, T., O'Dowd, C. D., and Seinfeld, J. H.: Iodine oxide homogeneous nucleation: An explanation for coastal new particle production, Geophys. Res. Lett., 28, 1949–1952, https://doi.org/10.1029/2000gl012399, 2001.

Hu, Q. J., Yu, P. R., Zhu, Y. J., Li, K., Gao, H. W., and Yao, X. H.: Concentration, Size Distribution, and Formation of Trimethylaminium and Dimethylaminium Ions in Atmospheric Particles over Marginal Seas of China*, J. Atmos. Sci., 72, 3487–3498, https://doi.org/10.1175/jas-d-14-0393.1, 2015.

Jokinen, T., Sipilä, M., Kontkanen, J., Vakkari, V., Tisler, P., Duplissy, E. M., Junninen, H., Kangasluoma, J., Manninen, H. E., Petäjä, T., Kulmala, M., Worsnop, D. R., Kirkby, J., Virkkula, A., and Kerminen, V. M.: Ion-induced sulfuric acid-ammonia nucleation drives particle formation in coastal Antarctica, Sci. Adv., 4, eaat9744, https://doi.org/10.1126/sciadv.aat9744, 2018.

Kalivitis, N., Kerminen, V.-M., Kouvarakis, G., Stavroulas, I., Bougiatioti, A., Nenes, A., Manninen, H. E., Petäjä, T., Kulmala, M., and Mihalopoulos, N.: Atmospheric new particle formation as a source of CCN in the eastern Mediterranean marine boundary layer, Atmos. Chem. Phys., 15, 9203–9215, https://doi.org/10.5194/acp-15-9203-2015, 2015.

Kirkby, J., Curtius, J., Almeida, J., Dunne, E., Duplissy, J., Ehrhart, S., Franchin, A., Gagné, S., Ickes, L., Kürten, A., Kupc, A., Metzger, A., Riccobono, F., Rondo, L., Schobesberger, S., Tsagkogeorgas, G., Wimmer, D., Amorim, A., Bianchi, F., Breitenlechner, M., David, A., Dommen, J., Downard, A., Ehn, M., Flagan, R. C., Haider, S., Hansel, A., Hauser, D., Jud, W., Junninen, H., Kreissl, F., Kvashin, A., Laaksonen, A., Lehtipalo, K., Lima, J., Lovejoy, E. R., Makhmutov, V., Mathot, S., Mikkilä, J., Minginette, P., Mogo, S., Nieminen, T., Onnela, A., Pereira, P., Petäjä, T., Schnitzhofer, R., Seinfeld, J. H., Sipilä, M., Stozhkov, Y., Stratmann, F., Tomé, A., Vanhanen, J., Viisanen, Y., Vrtala, A., Wagner, P. E., Walther, H., Weingartner, E., Wex, H., Winkler, P. M., Carslaw, K. S., Worsnop, D. R., Baltensperger, U., and Kulmala, M.: Role of sulphuric acid, ammonia and galactic cosmic rays in atmospheric aerosol nucleation, Nature, 476, 429–U477, https://doi.org/10.1038/nature10343, 2011.

Knattrup, Y. and Elm, J.: Clusteromics IV: The Role of Nitric Acid in Atmospheric Cluster Formation, Acs Omega, 7, 31551–315560, https://doi.org/10.1021/acsomega.2c04278, 2022.

Kubecka, J., Besel, V., Kurtén, T., Myllys, N., and Vehkamäki, H.: Configurational Sampling of Noncovalent (Atmospheric) Molecular Clusters: Sulfuric Acid and Guanidine, J. Phys. Chem. A, 123, 6022–6033, https://doi.org/10.1021/acs.jpca.9b03853, 2019.

Kurfman, L. A., Odbadrakh, T. T., and Shields, G. C.: Calculating Reliable Gibbs Free Energies for Formation of Gas-Phase Clusters that Are Critical for Atmospheric Chemistry: $(H_2SO_4)_3$, J. Phys. Chem. A, 125, 3169–3176, https://doi.org/10.1021/acs.jpca.1c00872, 2021.

Kürten, A., Li, C., Bianchi, F., Curtius, J., Dias, A., Donahue, N. M., Duplissy, J., Flagan, R. C., Hakala, J., Jokinen, T., Kirkby, J., Kulmala, M., Laaksonen, A., Lehtipalo, K., Makhmutov, V., Onnela, A., Rissanen, M. P., Simon, M., Sipilä, M., Stozhkov, Y., Tröstl, J., Ye, P., and McMurry, P. H.: New particle formation in the sulfuric acid–dimethylamine–water system: reevaluation of CLOUD chamber measurements and comparison to an aerosol nucleation and growth model, Atmos. Chem. Phys., 18, 845–863, https://doi.org/10.5194/acp-18-845-2018, 2018.

Kurtén, T., Loukonen, V., Vehkamäki, H., and Kulmala, M.: Amines are likely to enhance neutral and ion-induced sulfuric acid-water nucleation in the atmosphere more effectively than ammonia, Atmos. Chem. Phys., 8, 4095–4103, https://doi.org/10.5194/acp-8-4095-2008, 2008.

Lee, S.-H., Gordon, H., Yu, H., Lehtipalo, K., Haley, R., Li, Y., and Zhang, R.: New Particle Formation in the Atmosphere: From Molecular Clusters to Global Climate, J. Geophys. Res.-Atmos., 124, 7098–7146, https://doi.org/10.1029/2018jd029356, 2019.

Liu, L., Li, H., Zhang, H. J., Zhong, J., Bai, Y., Ge, M. F., Li, Z. S., Chen, Y., and Zhang, X. H.: The role of nitric acid in atmospheric new particle formation, Phys. Chem. Chem. Phys., 20, 17406–17414, https://doi.org/10.1039/c8cp02719f, 2018.

Liu, L., Yu, F. Q., Du, L., Yang, Z., Francisco, J. S., and Zhang, X. H.: Rapid sulfuric acid-dimethylamine nucleation enhanced by nitric acid in polluted regions, P. Natl. Acad. Sci. USA, 118, e2108384118, https://doi.org/10.1073/pnas.2108384118, 2021a.

Liu, L., Yu, F., Tu, K., Yang, Z., and Zhang, X.: Influence of atmospheric conditions on the role of trifluoroacetic acid in atmospheric sulfuric acid–dimethylamine nucleation, Atmos. Chem. Phys., 21, 6221–6230, https://doi.org/10.5194/acp-21-6221-2021, 2021b.

Liu, L., Li, S., Zu, H., and Zhang, X.: Unexpectedly significant stabilizing mechanism of iodous acid on iodic acid nucleation under different atmospheric conditions, Sci. Total Environ., 859, 159832, https://doi.org/10.1016/j.scitotenv.2022.159832, 2023.

Liu, Z. Y., Li, M., Wang, X. F., Liang, Y. H., Jiang, Y. R., Chen, J., Mu, J. S., Zhu, Y. J., Meng, H., Yang, L. X., Hou, K. Y., Wang, Y. F., and Xue, L. K.: Large contributions of anthropogenic sources to amines in fine particles at a coastal area in northern China in winter, Sci. Total Environ., 839, 156281, https://doi.org/10.1016/j.scitotenv.2022.156281, 2022.

Lu, T. and Chen, F.: Multiwfn: a multifunctional wavefunction analyzer, J. Comput. Chem., 33, 580–592, https://doi.org/10.1002/jcc.22885, 2012a.

Lu, T. and Chen, F.: Quantitative analysis of molecular surface based on improved Marching Tetrahedra algorithm, J. Mol. Graph. Model., 38, 314–323, https://doi.org/10.1016/j.jmgm.2012.07.004, 2012b.

Lu, Y. Q., Liu, L., Ning, A., Yang, G., Liu, Y. L., Kurten, T., Vehkamaki, H., Zhang, X. H., and Wang, L.: Atmospheric Sulfuric Acid-Dimethylamine Nucleation Enhanced by Trifluoroacetic Acid, Geophys. Res. Lett., 47, e2019GL085627, https://doi.org/10.1029/2019gl085627, 2020.

Ma, F. F., Xie, H. B., Zhang, R. J., Su, L. H., Jiang, Q., Tang, W. H., Chen, J. W., Engsvang, M., Elm, J., and He, X. C.: Enhancement of Atmospheric Nucleation Precursors on Iodic Acid- Induced Nucleation: Predictive Model and Mechanism, Environ. Sci. Technol., 57, 6944–6954, https://doi.org/10.1021/acs.est.3c01034, 2023.

Mahajan, A. S., Sorribas, M., Gómez Martín, J. C., MacDonald, S. M., Gil, M., Plane, J. M. C., and Saiz-Lopez, A.: Concurrent observations of atomic iodine, molecular iodine and ultrafine particles in a coastal environment, Atmos. Chem. Phys., 11, 2545–2555, https://doi.org/10.5194/acp-11-2545-2011, 2011.

McFiggans, G., Bale, C. S. E., Ball, S. M., Beames, J. M., Bloss, W. J., Carpenter, L. J., Dorsey, J., Dunk, R., Flynn, M. J., Furneaux, K. L., Gallagher, M. W., Heard, D. E., Hollingsworth, A. M., Hornsby, K., Ingham, T., Jones, C. E., Jones, R. L., Kramer, L. J., Langridge, J. M., Leblanc, C., LeCrane, J.-P., Lee, J. D., Leigh, R. J., Longley, I., Mahajan, A. S., Monks, P. S., Oetjen, H., Orr-Ewing, A. J., Plane, J. M. C., Potin, P.,

Shillings, A. J. L., Thomas, F., von Glasow, R., Wada, R., Whalley, L. K., and Whitehead, J. D.: Iodine-mediated coastal particle formation: an overview of the Reactive Halogens in the Marine Boundary Layer (RHaMBLe) Roscoff coastal study, Atmos. Chem. Phys., 10, 2975–2999, https://doi.org/10.5194/acp-10-2975-2010, 2010.

McGrath, M. J., Olenius, T., Ortega, I. K., Loukonen, V., Paasonen, P., Kurtén, T., Kulmala, M., and Vehkamäki, H.: Atmospheric Cluster Dynamics Code: a flexible method for solution of the birth-death equations, Atmos. Chem. Phys., 12, 2345–2355, https://doi.org/10.5194/acp-12-2345-2012, 2012.

Müller, C., Iinuma, Y., Karstensen, J., van Pinxteren, D., Lehmann, S., Gnauk, T., and Herrmann, H.: Seasonal variation of aliphatic amines in marine sub-micrometer particles at the Cape Verde islands, Atmos. Chem. Phys., 9, 9587–9597, https://doi.org/10.5194/acp-9-9587-2009, 2009.

Murphy, D. M. and Ravishankara, A. R.: Trends and patterns in the contributions to cumulative radiative forcing from different regions of the world, P. Natl. Acad. Sci. USA, 115, 13192–13197, https://doi.org/10.1073/pnas.1813951115, 2018.

Nault, B. A., Campuzano-Jost, P., Day, D. A., Jo, D. S., Schroder, J. C., Allen, H. M., Bahreini, R., Bian, H. S., Blake, D. R., Chin, M., Clegg, S. L., Colarco, P. R., Crounse, J. D., Cubison, M. J., DeCarlo, P. F., Dibb, J. E., Diskin, G. S., Hodzic, A., Hu, W. W., Katich, J. M., Kim, M. J., Kodros, J. K., Kupc, A., Lopez-Hilfiker, F. D., Marais, E. A., Middlebrook, A. M., Neuman, J. A., Nowak, J. B., Palm, B. B., Paulot, F., Pierce, J. R., Schill, G. P., Scheuer, E., Thornton, J. A., Tsigaridis, K., Wennberg, P. O., Williamson, C. J., and Jimenez, J. L.: Chemical transport models often underestimate inorganic aerosol acidity in remote regions of the atmosphere, Commun. Earth Environ., 2, 93, https://doi.org/10.1038/s43247-021-00164-0, 2021.

Ning, A., Liu, L., Zhang, S. B., Yu, F. Q., Du, L., Ge, M. F., and Zhang, X. H.: The critical role of dimethylamine in the rapid formation of iodic acid particles in marine areas, NPJ Clim. Atmos. Sci., 5, 92, https://doi.org/10.1038/s41612-022-00316-9, 2022.

O'Dowd, C. D. and de Leeuw, G.: Marine aerosol production: a review of the current knowledge, Philos. Trans. A Math. Phys. Eng. Sci., 365, 1753–1774, https://doi.org/10.1098/rsta.2007.2043, 2007.

O'Dowd, C. D., Hämeri, K., Mäkelä, J., Väkeva, M., Aalto, P., de Leeuw, G., Kunz, G. J., Becker, E., Hansson, H. C., Allen, A. G., Harrison, R. M., Berresheim, H., Geever, M., Jennings, S. G., and Kulmala, M.: Coastal new particle formation:: Environmental conditions and aerosol physicochemical characteristics during nucleation bursts, J. Geophys. Res.-Atmos., 107, 8107, https://doi.org/10.1029/2000jd000206, 2002a.

O'Dowd, C. D., Hämeri, K., Mäkelä, J. M., Pirjola, L., Kulmala, M., Jennings, S. G., Berresheim, H., Hansson, H.-C., de Leeuw, G., Kunz, G. J., Allen, A. G., Hewitt, C. N., Jackson, A., Viisanen, Y., and Hoffmann, T.: A dedicated study of new particle formation and fate in the coastal environment: overview of objectives and achievements, J. Geophys. Res.-Atmos., 107, 1–16, https://doi.org/10.1029/2001jd000555, 2002b.

O'Dowd, C. D., Jimenez, J. L., Bahreini, R., Flagan, R. C., Seinfeld, J. H., Hämeri, K., Pirjola, L., Kulmala, M., Jennings, S. G., and Hoffmann, T.: Marine aerosol formation from biogenic iodine emissions, Nature, 417, 632–636, https://doi.org/10.1038/nature00775, 2002c.

Olenius, T., Halonen, R., Kurtén, T., Henschel, H., Kupiainen-Määtä, O., Ortega, I. K., Jen, C. N., Vehkamäki, H., and Riipinen, I.: New particle formation from sulfuric acid and amines: Comparison of monomethylamine, dimethylamine, and trimethylamine, J. Geophys. Res.-Atmos., 122, 7103–7118, https://doi.org/10.1002/2017jd026501, 2017.

Peterson, K. A.: Systematically convergent basis sets with relativistic pseudopotentials. I. Correlation consistent basis sets for the post-d group 13–15 elements, The J. Chem. Phys., 119, 11099–11112, https://doi.org/10.1063/1.1622923, 2003.

Pope III, C. A. and Dockery, D. W.: Health effects of fine particulate air pollution: lines that connect, J. Air Waste Manage. Assoc., 56, 709–742, https://doi.org/10.1080/10473289.2006.10464485, 2006.

Quéléver, L. L. J., Dada, L., Asmi, E., Lampilahti, J., Chan, T., Ferrara, J. E., Copes, G. E., Pérez-Fogwill, G., Barreira, L., Aurela, M., Worsnop, D. R., Jokinen, T., and Sipilä, M.: Investigation of new particle formation mechanisms and aerosol processes at Marambio Station, Antarctic Peninsula, Atmos. Chem. Phys., 22, 8417–8437, https://doi.org/10.5194/acp-22-8417-2022, 2022.

Rappé, A. K., Casewit, C. J., Colwell, K. S., Goddard, W. A., and Skiff, W. M.: UFF, a Full Periodic-Table Force-Field for Molecular Mechanics and Molecular-Dynamics Simulations, J. Am. Chem. Soc., 114, 10024–10035, https://doi.org/10.1021/ja00051a040, 1992.

Rong, H., Liu, J., Zhang, Y., Du, L., Zhang, X., and Li, Z.: Nucleation mechanisms of iodic acid in clean and polluted coastal regions, Chemosphere, 253, 126743, https://doi.org/10.1016/j.chemosphere.2020.126743, 2020.

Schmitz, G.: Inorganic reactions of iodine(III) in acidic solutions and free energy of iodous acid formation, Int. J. Chem. Kinet., 40, 647–652, https://doi.org/10.1002/kin.20344, 2008.

Shampine, L. and Reichelt, M.: The MATLAB ODE suite, SIAM J. Sci. Comput., 18, 1–22, https://doi.org/10.1137/S1064827594276424, 1997.

Shen, J. W., Elm, J., Xie, H. B., Chen, J. W., Niu, J. F., and Vehkamäki, H.: Structural Effects of Amines in Enhancing Methanesulfonic Acid-Driven New Particle Formation, Environ. Sci. Technol., 54, 13498–13508, https://doi.org/10.1021/acs.est.0c05358, 2020.

Sipilä, M., Sarnela, N., Jokinen, T., Henschel, H., Junninen, H., Kontkanen, J., Richters, S., Kangasluoma, J., Franchin, A., Peräkylä, O., Rissanen, M. P., Ehn, M., Vehkamäki, H., Kurten, T., Berndt, T., Petäjä, T., Worsnop, D., Ceburnis, D., Kerminen, V. M., Kulmala, M., and O'Dowd, C.: Molecular-scale evidence of aerosol particle formation via sequential addition of HIO_3, Nature, 537, 532–534, https://doi.org/10.1038/nature19314, 2016.

Stewart, J. J.: Stewart Computational Chemistry, Colorado Springs, CO, USA, http://openmopac.net/MOPAC2016.html (last access: 12 May 2024), 2016.

Stewart, J. J. P.: Optimization of parameters for semiempirical methods VI: more modifications to the NDDO approximations and re-optimization of parameters, J. Molecul. Model., 19, 1–32, https://doi.org/10.1007/s00894-012-1667-x, 2013.

Vanneste, A., Duce, R. A., and Lee, C.: Methylamines in the marine atmosphere, Geophys. Res. Lett., 14, 711–714, https://doi.org/10.1029/GL014i007p00711, 1987.

Wang, J. Y., Xu, G. J., Chen, L. Q., and Chen, K.: Atmospheric Particle Number Concentrations and New Particle Formation over the Southern Ocean and Antarctica: A Critical Review, Atmosphere, 14, 402, https://doi.org/10.3390/atmos14020402, 2023.

Wang, M. Y., Kong, W. M., Marten, R., He, X. C., Chen, D. X., Pfeifer, J., Heitto, A., Kontkanen, J., Dada, L., Kurten, A., Yli-Juuti, T., Manninen, H. E., Amanatidis, S., Amorim, A., Baalbaki, R., Baccarini, A., Bell, D. M., Bertozzi, B., Bräkling, S., Brilke, S., Murillo, L. C., Chiu, R., Chu, B. W., De Menezes, L. P., Duplissy, J., Finkenzeller, H., Carracedo, L. G., Granzin, M., Guida, R., Hansel, A., Hofbauer, V., Krechmer, J., Lehtipalo, K., Lamkaddam, H., Lampimäki, M., Lee, C. P., Makhmutov, V., Marie, G., Mathot, S., Mauldin, R. L., Mentler, B., Muller, T., Onnela, A., Partoll, E., Petäjä, T., Philippov, M., Pospisilova, V., Ranjithkumar, A., Rissanen, M., Rörup, B., Scholz, W., Shen, J. L., Simon, M., Sipilä, M., Steiner, G., Stolzenburg, D., Tham, Y. J., Tomé, A., Wagner, A. C., Wang, D. Y. S., Wang, Y. H., Weber, S. K., Winkler, P. M., Wlasits, P. J., Wu, Y. H., Xiao, M., Ye, Q., Zauner-Wieczorek, M., Zhou, X. Q., Volkamer, R., Riipinen, I., Dommen, J., Curtius, J., Baltensperger, U., Kulmala, M., Worsnop, D. R., Kirkby, J., Seinfeld, J. H., El-Haddad, I., Flagan, R. C., and Donahue, N. M.: Rapid growth of new atmospheric particles by nitric acid and ammonia condensation, Nature, 581, 184–189, https://doi.org/10.1038/s41586-020-2270-4, 2020.

Wang, M. Y., Xiao, M., Bertozzi, B., Marie, G., Rörup, B., Schulze, B., Bardakov, R., He, X. C., Shen, J. L., Scholz, W., Marten, R., Dada, L., Baalbaki, R., Lopez, B., Lamkaddam, H., Manninen, H. E., Amorim, A., Ataei, F., Bogert, P., Brasseur, Z., Caudillo, L., De Menezes, L. P., Duplissy, J., Ekman, A. M. L., Finkenzeller, H., Carracedo, L. G., Granzin, M., Guida, R., Heinritzi, M., Hofbauer, V., Höhler, K., Korhonen, K., Krechmer, J. E., Kürten, A., Lehtipalo, K., Mahfouz, N. G. A., Makhmutov, V., Massabò, D., Mathot, S., Mauldin, R. L., Mentler, B., Müller, T., Onnela, A., Petäjä, T., Philippov, M., Piedehierro, A. A., Pozzer, A., Ranjithkumar, A., Schervish, M., Schobesberger, S., Simon, M., Stozhkov, Y., Tomé, A., Umo, N. S., Vogel, F., Wagner, R., Wang, D. S., Weber, S. K., Welti, A., Wu, Y. S., Zauner-Wieczorek, M., Sipilä, M., Winkler, P. M., Hansel, A., Baltensperger, U., Kulmala, M., Flagan, R. C., Curtius, J., Riipinen, I., Gordon, H., Lelieveld, J., El-Haddad, I., Volkamer, R., Worsnop, D. R., Christoudias, T., Kirkby, J., Möhler, O., and Donahue, N. M.: Synergistic HNO_3-H_2SO_4-NH_3 upper tropospheric particle formation, Nature, 605, 483–489, https://doi.org/10.1038/s41586-022-04605-4, 2022.

Weber, R. J., Marti, J. J., McMurry, P. H., Eisele, F. L., Tanner, D. J., and Jefferson, A.: Measured atmospheric new particle formation rates: Implications for nucleation mechanisms, Chem. Eng. Commun., 151, 53–64, https://doi.org/10.1080/00986449608936541, 1996.

Xia, D., Chen, J., Yu, H., Xie, H. B., Wang, Y., Wang, Z., Xu, T., and Allen, D. T.: Formation Mechanisms of Iodine-Ammonia Clusters in Polluted Coastal Areas Unveiled by Thermodynamic and Kinetics Simulations, Environ. Sci. Technol., 54, 9235–9242, https://doi.org/10.1021/acs.est.9b07476, 2020.

Xie, H. B. and Elm, J.: Tri-Base Synergy in Sulfuric Acid-Base Clusters, Atmosphere, 12, 1260, https://doi.org/10.3390/atmos12101260, 2021.

Yang, Y., Weaver, M. N., and Merz, K. M.: Assessment of the "6-31+G**+LANL2DZ" Mixed Basis Set Coupled with Density Functional Theory Methods and the Effective Core Potential: Prediction of Heats of Formation and Ionization Potentials for First-Row-Transition-Metal Complexes, J. Phys. Chem. A, 113, 9843–9851, https://doi.org/10.1021/jp807643p, 2009.

Yang, Y., Waller, S. E., Kreinbihl, J. J., and Johnson, C. J.: Direct Link between Structure and Hydration in Ammonium and Aminium Bisulfate Clusters Implicated in Atmospheric New Particle Formation, J. Phys. Chem. Lett., 9, 5647–5652, https://doi.org/10.1021/acs.jpclett.8b02500, 2018.

Yao, L., Garmash, O., Bianchi, F., Zheng, J., Yan, C., Kontkanen, J., Junninen, H., Mazon, S. B., Ehn, M., Paasonen, P., Sipila, M., Wang, M. Y., Wang, X. K., Xiao, S., Chen, H. F., Lu, Y. Q., Zhang, B. W., Wang, D. F., Fu, Q. Y., Geng, F. H., Li, L., Wang, H. L., Qiao, L. P., Yang, X., Chen, J. M., Kerminen, V. M., Petaja, T., Worsnop, D. R., Kulmala, M., and Wang, L.: Atmospheric new particle formation from sulfuric acid and amines in a Chinese megacity, Science, 361, 278–281, https://doi.org/10.1126/science.aao4839, 2018.

Yu, F. and Luo, G.: Modeling of gaseous methylamines in the global atmosphere: impacts of oxidation and aerosol uptake, Atmos. Chem. Phys., 14, 12455–12464, https://doi.org/10.5194/acp-14-12455-2014, 2014.

Yu, H., Ren, L., Huang, X., Xie, M., He, J., and Xiao, H.: Iodine speciation and size distribution in ambient aerosols at a coastal new particle formation hotspot in China, Atmos. Chem. Phys., 19, 4025–4039, https://doi.org/10.5194/acp-19-4025-2019, 2019.

Zhang, J. and Dolg, M.: ABCluster: the artificial bee colony algorithm for cluster global optimization, Phys. Chem. Chem. Phys., 17, 24173–24181, https://doi.org/10.1039/C5CP04060D, 2015.

Zhang, M. M., Yan, J. P., Lin, Q., Park, K., Zhao, S. H., Xu, S. Q., and Wang, S. S.: Low contributions of dimethyl sulfide (DMS) chemistry to atmospheric aerosols over the high Arctic Ocean, Atmos. Environ., 313, 120073, https://doi.org/10.1016/j.atmosenv.2023.120073, 2023.

Zhang, R.: Getting to the Critical Nucleus of Aerosol Formation, Science, 328, 1366–1367, https://doi.org/10.1126/science.1189732, 2010.

Zhang, R., Khalizov, A., Wang, L., Hu, M., and Xu, W.: Nucleation and growth of nanoparticles in the atmosphere, Chem. Rev., 112, 1957–2011, https://doi.org/10.1021/cr2001756, 2012.

Zhang, R. J., Xie, H. B., Ma, F. F., Chen, J. W., Iyer, S., Simon, M., Heinritzi, M., Shen, J. L., Tham, Y. J., Kurten, T., Worsnop, D. R., Kirkby, J., Curtius, J., Sipila, M., Kulmala, M., and He, X. C.: Critical Role of Iodous Acid in Neutral Iodine Oxoacid Nucleation, Environ. Sci. Technol., 56, 14166–14177, https://doi.org/10.1021/acs.est.2c04328, 2022a.

Zhang, S. B., Li, S. N., Ning, A., Liu, L., and Zhang, X. H.: Iodous acid – a more efficient nucleation precursor than iodic acid, Phys. Chem. Chem. Phys., 24, 13651–13660, https://doi.org/10.1039/d2cp00302c, 2022b.

Zhu, Y., Li, K., Shen, Y., Gao, Y., Liu, X., Yu, Y., Gao, H., and Yao, X.: New particle formation in the marine atmosphere during seven cruise campaigns, Atmos. Chem. Phys., 19, 89–113, https://doi.org/10.5194/acp-19-89-2019, 2019.

Zu, H. T., Zhang, S. B., Liu, L., and Zhang, X. H.: The vital role of sulfuric acid in iodine oxoacids nucleation: impacts of urban pollutants on marine atmosphere, Environ. Res. Lett., 19, 014076, https://doi.org/10.1088/1748-9326/ad193f, 2024.